LAG3+ CD8+ T cell Subset Boosts Bispecific Antibody Armed Activated T Cell Cytotoxicity Directed at Hormone Receptor+ Breast Cancers

AUTHORS: *Robert Weldon Barnes[1,4], Archana Thakur [2], Suna Onengut-Gumuscu, [3], Lawrence G. Lum [2,5], Sepideh Dolatshahi.*[1,4,5]

[1]Department of Biomedical Engineering, University of Virginia (UVA) School of Medicine, Charlottesville, Virginia 22908

[2]Division of Hematology & Oncology, Department of Medicine, UVA School of Medicine

[3]Department of Genome Sciences, University of Virginia School of Medicine

[4]Beirne B. Carter Center for Immunology Research, UVA School of Medicine, Charlottesville, Virginia 22908

[5]University of Virginia Cancer Center, Charlottesville, Virginia, USA

KEYWORDS

Bispecific antibody armed T cell, Checkpoint Inhibitors, Systems Immunology, Therapeutic synergy, Mechanistic Modeling, Rational Design of Combination Therapies, LAG3, TIGIT, HR+/HER2- Breast Cancer.

DECLARATIONS

Ethics approval and consent to participate – Not applicable.

Consent for publication – Not applicable.

Availability of data and material – Computational modeling algorithms (OPLS-R) and the mechanistic model of BAT-tumor interactions (ODE model) are available on GitHub (https://github.com/Dolatshahi-Lab). All cytotoxicity and processed flow cytometry data will be provided as Supplemental tables. Raw flow cytometry data and CITE-seq data will be provided upon request.

Competing interests – LGL is cofounder of Transtarget Inc, Founder of BATs, LLC, member of SAB of Rapa Therapeutics and Tundra Targeted Therapeutics and consults for iCell Gene Therapeutics. AT is a cofounder of Alpha Immune LLC.

Funding – This work was funded by SD startup funds, UV Cancer Center Support Grant P30 CA044579 and LGL UVA startup funds. The UVA Comprehensive Cancer Center Support Grant (P30CA044579) from the NCI additionally supported work performed by the Genome Analysis and Technology Core, RRID:SCR_018883 and Biorepository and Tissue Research Facility, RRID:SCR_022971. This research was also supported by the UVA Farrow Fellowship.

Authors contributions – RWB, SD, and LGL were responsible for the conceptualization of the project and methodologies. RWB and SD wrote the manuscript with input from all authors. SD and LGL provided supervision. RWB performed experiments, analyzed data, and built the computational models. RWB, AT, SOG, LGL, and SD contributed to the design and development of the investigation. SD was responsible for funding acquisition. All authors approved the final version of the manuscript.

Acknowledgements – This work was presented at the 2024 Society for Immunotherapy of Cancer (SITC) annual meeting (Abstract #718). We thank the Dolatshahi lab members and Dr. Kristin Anderson for providing feedback.

Authors' information (optional) –

Robert W. Barnes– ORCID iD 0000-0001-6494-4033

Sepideh Dolatshahi – ORCID iD 0000-0003-0226-0933

Suna Onengut-Gumuscu – ORCID iD 0000-0002-6563-8334

Archana Thakur – ORCID iD 0000-0003-3876-9555

Lawrence G. Lum – ORCID iD 0000-0001-7561-6035

LIST OF ABBREVIATIONS – Tumor microenvironment, TME; Bispecific antibody armed T cell, BATs; checkpoint inhibitor, CPI; hormone receptor-positive, HR+; Lymphocyte activation gene 3, LAG3; Programmed Cell Death Protein 1, PD-1; T cell immunoreceptor with immunoglobulin and ITIM domain, TIGIT; bispecific antibodies, BiAb; overall survival, OS; metastatic breast cancer, MBC; ordinary differential equation, ODE; unarmed activated T cells, ATC; cellular indexing of transcriptomes and epitopes, CITE-seq; real-time cell analysis, RTCA; orthogonalized partial least squares regression, OPLS-R; variable importance in projection, VIP; uniform manifold approximation and projection, UMAP; T cell receptor, TCR.

What is already known on this topic – Bispecific antibody armed T cell (BATs) therapies are adoptive T cell therapies that can effectively reroute T cell cytotoxicity toward cancerous cells, but lack consistent and durable anti-tumor responses. Checkpoint proteins expressed on the surface of activated T cells dampen immune responses and can be overstimulated in solid tumors to hamper tumor clearance by T cells. Checkpoint inhibitor drugs can improve T cell anti-tumor response by blocking checkpoint protein signaling but are only effective if the targeted checkpoint protein is expressed on the T cell and activated in the tumor microenvironment, highlighting an opportunity to enhance BAT efficacy by combining treatment with synergistic CPI.

What this study adds – This study characterizes dynamic, time-resolved patterns in checkpoint protein expression by breast cancer-targeting adoptive T cells and predicts the significance of high-prevalence checkpoint proteins on T cell function. It also demonstrates the use of multivariate statistic and mathematical modeling toward rational design of targets and timing strategies for synergistic combination therapies.

How this study might affect research, practice, or policy – The output of this study provides justification for therapeutic strategies combining adoptive T cell therapies with checkpoint inhibitor drugs targeting TIGIT and LAG3 as a means of improving patient responses in HER2-/HR+ breast cancers.

ABSTRACT

Tumor clearance by T cells is impaired by insufficient tumor antigen recognition, insufficient tumor infiltration, and the immunosuppressive tumor microenvironment (TME). Although targeted T cell therapy circumvents failures in tumor antigen recognition, suppression by the TME and failure to infiltrate the tumor can hinder tumor clearance by these T cells. Checkpoint inhibitors (CPI) promises to reverse T cell suppression in the TME and can be combined with bispecific antibody armed T cell (BATs) therapy to improve clinical outcomes. CPIs require the target pathway of inhibition to be active in the TME to elicit a therapeutic response. We hypothesize that adoptively transferred T cell function may be improved by the addition of CPI if the inhibitory pathway is functionally active. This study develops a kinetic-dynamic model of serial killing of hormone receptor-positive (HR+) breast cancer cells mediated by BATs using single-cell transcriptomic and

temporal protein data to identify T cell phenotypes and quantify inhibitory receptor expression. LAG3, PD-1, and TIGIT were identified as inhibitory receptors expressed by cytotoxic effector CD8 BATs upon exposure to HR+ breast cancer cell lines. These data were combined with real-time tumor cytotoxicity data in a multivariate statistical analysis framework to predict the relevant contributions of T cells expressing each receptor to tumor reduction. A mechanistic kinetic-dynamic mathematical model was developed and parametrized using protein expression and cytotoxicity data for in silico validation of the findings of the multivariate statistical analysis. The model corroborated the predictions of the multivariate statistical analysis which identified LAG3+ BATs as the primary effectors, while TIGIT expression dampened cytotoxic function. These results inform CPI selection for BATs combination therapy and provide a framework to maximize BATs anti-tumor function against HR+ cancers. Our model provides a means to optimize targets for CPIs used in combination with BATs in clinical strategies.

BACKGROUND

HR+/HER2- breast cancers represent 68% of all breast cancer diagnoses[1]. Targeted adoptive T cell therapies offer an effective approach to elicit T cell immune responses against tumors lacking a sufficiently recognizable tumor antigen[2–6]. Bispecific antibody-armed activated T-cell (BATs) therapies utilize activated T cells armed with bispecific antibodies (BiAb) targeting CD3 and a tumor antigen to redirect non-MHC restricted T cell cytotoxicity toward high and low antigen expressing cancer cells[6,7]. This strategy has shown encouraging results in reducing tumor burden, improving quality of

life, and improving median overall survival (OS) in patients with stage IV breast[8,9], prostate[10], and pancreatic[5] cancers and neuroblastoma[11].

In a phase I trial involving 17 heavily pretreated HER2-/HR+ metastatic breast cancer (MBC) patients, HER2 BATs therapy achieved a median OS of 27.4 months with 59% patients exhibiting stable disease at 14.5 weeks[12]. Similarly, a phase II trial with 24 HER2-/HR+ MBC patients reported a decrease in tumor markers in 56.5% of patients and a median OS of 15.2 months following HER2 BATs infusions[13]. Despite these successes, the lack of consistent and durable anti-tumor responses highlights an opportunity to enhance BAT efficacy by combining treatment with synergistic T cell targeting therapies.

Checkpoint inhibitors improve T cell function against solid tumors by preventing inhibitory signaling. While CPIs have shown efficacy in some breast cancers, response rates in HER2-/HR+ patients remain disappointingly low (5-12%) compared to HER2+ or TNBC patients[14–16]. CPI efficacy depends on the presence of the target protein and its complimentary ligands or receptors, suggesting that identifying reliable CPI targets in HER2-/HR+ tumors could improve therapeutic outcomes [17,18]. By characterizing inhibitory receptor expression dynamics and BATs function, this study investigates whether the timing and selection of CPI targets can provide an opportunity for the synergistic use of CPIs with BATs therapies for HR+/HER2- patients.

Computational modeling integrates diverse measurements to provide insights into how cellular changes affect therapeutic outcomes. Network modeling has revealed therapeutically targetable gene expression mechanisms governing T cell fate selection, function, and exhaustion20–23, but lacks temporal resolution and cannot account for repeated T cell stimulation in targeted cell therapies. Existing mechanistic models of

143 adoptive T cell therapies have described the emergence of T cell functional states[21–23],
144 but do not address therapeutic dysfunction.

145 To address this gap in knowledge, we developed a dynamic ordinary differential
146 equation (ODE) model that incorporates BATs inhibitory receptor expression profiles. This
147 model predicts the cytotoxic function of each BATs subset and can serve as an *in-silico*
148 testbed to optimize the synergistic use of CPI therapies by targeting the most functional
149 receptors at their peak expression time.

150 Using single-cell transcriptomics and temporal protein and gene expression data,
151 we characterized T cell phenotype emergence and receptor expression dynamics. These
152 data, combined with tumor cytotoxicity profiles, were analyzed using a multivariate
153 statistical framework to predict the relative contributions of BATs subspecies to tumor
154 cytotoxicity.

155 Our ODE model of BATs-mediated tumor killing was constructed from matched
156 temporal protein expression and cytotoxicity data to validate our multivariate analysis
157 findings. Both our multivariate statistical analysis and kinetic-dynamic model identified the
158 LAG3+ BATs subset as a key driver of tumor reduction across multiple donors and cancer
159 cell lines. These results suggest targeting LAG3 in BATs-CPI combinatorial therapies
160 could significantly improve therapeutic outcomes in HR+/HER2- breast cancer patients.

161

162 **METHODS**

163 **Target cell coculture**

164 MCF-7, CAMA1, and T47D cells were acquired from ATCC. Cells were thawed in the
165 media suggested by the manufacturer. MCF-7 cells were passaged in cRPMI (RPMI1640

166 + 10%FBS). CAMA1 and T47D cells were gradually acclimated to cRPMI by subsequent
167 passages in mixed (RPMI/native) media with gradually increasing RPMI proportions.
168 Cells were passaged every 2-3 days to avoid confluence.
169

170 **ATC generation**

171 Activated T cells (ATC) were generated using T cells collected from donor PBMC. Blood
172 was collected from normal donors and PBMC were obtained by Ficoll-Paque density
173 gradient separation, counted, suspended in RPMI supplemented with 100 U/mL IL-2 and
174 20 ng/mL OKT3 to activate T cells and stimulate proliferation[24]. T cells were expanded by
175 refreshing the cultures with RPMI containing 100 U of IL-2/mL every 2-3 days for 14 days.
176 The expanded T cells were harvested and cryopreserved at $100e^6$ viable cells (vc)/mL at
177 -160°C in LN2 until use.
178

179 **BATs preparation**

180 BATs were prepared as described[25]. ATC were thawed at 37°C, resuspended in RPMI,
181 and washed 2x in RPMI. Washed ATC were resuspended in RPMI + 50 ng/10^6 vc anti-
182 HER2x anti-CD3 bispecific antibody (HER2Bi) to generate HER2 BATs[26].
183

184 **Single-cell CITE-seq Analysis**

185 ATCs from 3 donors were thawed and split into two groups per donor. One group from
186 each donor was armed as described above to generate BATs. Each group was cocultured
187 for 1 hours with MCF7 tumor cells at a 10:1 BAT:MCF7 ratio. BATs were then collected
188 and measured using 10X Genomics CITE-seq technology[26]. TotalSeq^{TM}-B

189 oligonucleotide-labeled antibodies for CD45RO, CD45RA, CD3, CD4, CD8, CD69, and
190 CD25 were included in the CITE-seq panel, and cells were stained following the
191 manufacturer's protocol (BioLegend). CITE-seq libraries were processed in parallel
192 following 10X Genomics Single Cell 3' protocol and sequenced on an Illumina NextSeq
193 500.
194 Raw protein tag and transcriptomic data from each donor were integrated into a Seurat
195 object using the Seurat 5.0 R package[27]. Each object was filtered to remove cells with <
196 500 features or > 2500 features, as well as those with < 1% or > 5% mitochondrial DNA.
197 Data within each object was normalized and the 3000 most variable features were
198 identified. All 6 objects were integrated into a single object using Seurat
199 FindIntegrationAnchors and IntegrateData functions. Data was then scaled, and a
200 principal component analysis (PCA) was conducted to identify the top 100 principal
201 components (PCs). A K nearest-neighbor graph was constructed using the top 25 PCs
202 and used to identify cell clusters. A uniform manifold approximation and projection
203 (UMAP) plot for visualization was created using these clusters. Differential gene
204 expression was used to identify T cell clusters. Briefly, a Wilcoxon Ranked Sum test was
205 run using Seurat's FindAllMarkers function. Genes strongly differentiating each cluster
206 were cross-referenced with T cell literature to identify the phenotype in question.
207

208 **Real-time cell analysis (RTCA) measurements**

209 The xCelligence RTCA monitor was used to measure tumor cell death across the course
210 of the assay. xCelligence plates were zeroed with RPMI prior to seeding[28]. In brief, 2e4
211 vc target breast cancer cell lines were added to each xCelligence well and allowed to

212 adhere. The seeded plate was returned to the xCelligence RTCA monitor, and
213 conductivity readings were begun. After 24 hours, BATs were added to each well at
214 predefined ratios between 0.125 – 2 BATs:Tumor. As a surrogate for cytotoxicity,
215 conductivity measurements were recorded continuously for 120h.
216

217 **BATs coculture preparation**

218 Time-course samples were prepared by coculturing BATs and tumor cells at an effector:
219 target ratio of 1:1. Flat bottom 24 well plates were seeded with MCF-7 cells in RPMI at
220 1.2e5 vc/mL and incubated for 24 hours. After 24h, BATs were added at a E:T as
221 determined by target cell counts from a sample plate. Bat-tumor cocultures were
222 incubated for up to 72 hours. Samples were collected from wells at 4, 24, 48, and 72
223 hours. Collected samples were used for flow cytometry readings.
224

225 **Flow Cytometry**

226 Flow cytometry stain panels (**Table 1**) were created by mixing fluorescence-conjugated
227 antibody stains targeting the ligands of interest. The following panels were generated:
228 Inhibitory (CD45, CD4, CD8, TIGIT, PD-
229 1, LAG3, TIM-3, CTLA, BTLA),
230 Stimulatory (CD45, CD4, CD8, 4-1BB,
231 CD27, OX40, GITR, HVEM, LIGHT,
232 ICOS), and Coexpression (CD45, CD4,
233 CD8, 4-1BB, 4-1BBL, OX40, TIGIT, PD-
234 1, LAG3). Cells were resuspended,

Inhibitory Panel	Coexpression Panel	Stimulatory Panel
CD3	CD45	CD45
CD4	CD4	CD4
CD8	CD8	CD8
CTLA4	OX40	OX40
BTLA	4-1BBL	LIGHT
PD-1	PD-1	ICOS
TIGIT	TIGIT	HVEM
LAG3	LAG3	CD27
TIM-3	4-1BB	4-1BB
-	-	GITR

Table 1: Targets for fluorescent antibodies included in each flow cytometry panel.

235 counted for viability, stained, and fixed before fluorescent intensity readings were
236 acquired on the NovoCyte 3005 3 laser cytometer. Collected data was compensated and
237 analyzed using FlowJo flow cytometry data analysis software.
238
239 **OPLS-R analysis**
240 An orthogonalized partial least squares (OPLS)-regression model was built to predict the
241 impact of BATs receptor expression on tumor reduction. BATs were binned into distinct
242 groups by their expression of CD8 and CD4, and again by their expression of PD-1, TIGIT,
243 and/or LAG3. Triplicate counts were averaged within donor and against target cell line.
244 These counts were inputted to predict the changes in tumor cell count and the rate of
245 change in tumor counts as measured by RTCA. Separate models were created for the 3-
246 donor study and the 3-target study.
247 Inputs for tumor counts or rate of change compared against BATs counts were taken at
248 a set time interval from the time of BATs collection. Models for each study were created
249 with 0, 1, 4, 12, and 24-hour intervals from the time of BATs collection to increase the
250 robustness of model predictions. The variable importance in projection (VIP) scores for
251 each BATs subset were calculated[29], ranked, and artificially oriented in the direction of
252 their loadings on latent variable 1 (LV1). The directionality of groups with VIP scores >1
253 was used to predict the positive or negative impact on tumor growth for each
254 receptor/ligand.
255
256 **ODE model construction and testing**

257 An ODE model was constructed using mass action equations to describe changes in
258 tumor cell count. The following equation was used to describe tumor cell count.

259 $$\frac{dTumor}{dt} = a_{TP} * Tumor - \frac{a_{TP} * Tumor^2}{Max_{Tumor}} - \left(a_{Kill_N} * NBATs * Tumor\right)$$

260 $$- \left(a_{Kill_L} * LBATs * Tumor\right) - \left(a_{Kill_P} * PBATs * Tumor\right)$$

261 $$- \left(a_{KillD} * DBATs * Tumor\right)$$

262 The first term represents tumor growth in the absence of BATs, and the next four negative
263 terms represent the contribution of each BAT subset to the rate of tumor cell clearance.
264 Tumor growth rate was assumed to be sigmoidal, and was fit to data collected from the
265 control 0:1 BATs:Tumor condition during the RTCA experiment. NBATs, PBATs, LBATs,
266 and DBATs rate of change were determined by taking the derivative of spline functions fit
267 to the flow cytometry cell counts collected at 0, 4, 24, 48, and 72 hours.
268 The CaliPro parameter optimization package was used to determine the potential ranges
269 and optimal values for each species rate parameter [30]. CaliPro optimizes unknown model
270 parameters by creating a parameter space using Latin Hypercube Sampling within
271 parameter-specific ranges set by the user. Each parameter was tested by software, and
272 parameter sets that meet a user-defined set of criteria are used to generate a new LHS
273 parameter space for a second iteration. This procedure continued until a large enough
274 portion of parameters met the acceptance criteria. The final parameter space contains a
275 refined range of parameters which best describe the system in question. Acceptable
276 parameter spaces were those that generated tumor counts within +/- 10% of the
277 measured values at 0, 4, 12, 24 ,36, 48, 60, and 72 hours.
278
279

280 **RESULTS**

281 **Bispecific antibody-driven interactions generate highly cytotoxic LAG3+ effector T**
282 **cell populations after 1 hour exposure to target cells**

283 As a means of identifying phenotypic changes in T cells driven by the engagement of T
284 cell receptor (TCR) and tumor antigen mediated by the BiAb, we profiled transcriptional
285 and protein expression changes in HER2 BATs and unarmed ATCs after exposure to
286 tumor cells using cellular indexing of transcriptomes and epitopes by sequencing (CITE-
287 seq) (**Fig. 1A**). The matched protein and RNA data were integrated and pooled, and an
288 unsupervised graph-based clustering method was applied to generate 12 cell clusters
289 (**Fig 1B**). CD4 and CD8 protein tags were used to identify major T cell populations, while
290 CD69, CD45RA, and CD45RO protein tags helped differentiate between resting, dividing,
291 and activated T cell subsets (**Fig. 1B, Fig. S1**). These 12 cell subsets exhibited varying
292 transcriptomic expression profiles of cytotoxic factors, inhibitory receptors, costimulatory
293 receptors, and relevant transcription factors (**Fig. 1D**). Wilcoxon ranked-sum testing was
294 used to identify marker genes distinguishing each group (**Fig 1C**) to assist in applying
295 known T cell phenotypes.

296 The presence of the BiAb drove phenotypic changes in both CD4 and CD8 T cells (**Fig**
297 **1A, B**). Activated CD4 BATs, indicated by CD69 protein expression, switched primarily to
298 a pro-inflammatory T helper 1 (Th1) phenotype (**Fig 1C**, **Fig S1**). A smaller subset of
299 activated CD4 BATs was observed to adopt a humoral Th2 phenotype (**Fig 1B**), which
300 not only drives B cells to produce immunoglobulins but may also facilitate tumor
301 progression[31]. The Th1 population was comprised primarily of BATs, which accounted for
302 82% of the population, while the Th2 population was evenly split between BATs (46%)

303 and ATC (54%). CD8 BATs displayed progressive activation: a mid-activation group,
304 labeled CD8_Act, was CD45RO+CD69+, while a fully activated effector group, labeled
305 CD8_Eff, was CD45RA+CD69+. Additionally, two smaller BATs groups, an NK-like (NKT)
306 group marked by KLRD1[32] and FCER1G[33] and mucosal-associated invariant (MAIT)
307 group marked by KLRB1[34] and NCR3[35], were also present. The CD8_Eff group was
308 identified as the primary cytotoxic group, as demonstrated by high expression of
309 granzyme (GZMA, GZMB, GZMK, GZMH) and perforin (PRF) genes, as well as
310 inflammatory cytokine (IFN-γ, TNF-α) and FAS ligand expression (**Fig 1D**). The CD8_Eff
311 group was also enriched in EOMES and TBX21, two transcriptional regulators associated
312 with T cell maturation, terminal differentiation, and effector function[36], further indicating
313 the role of this group as an effector T cell (**Fig 1D**). TCF7, a transcriptional regulator
314 indicating a pre-antigen encounter T cell state[37], was downregulated in the CD8_Eff
315 group, while TOX, a gene associated with T cell effector function and exhaustion[38], was
316 upregulated (**Fig 1D**).
317 Strong cytotoxic potential was observed to correlate with targetable inhibitory and
318 costimulatory receptor expression (**Fig 1D**). The cosignaling receptors LAG3 and TIGIT,
319 which directly modulate BATs cytotoxicity, were enriched in the CD8_Eff group (**Fig 1E**).
320 While expression of PD-1 (PDCD1), TIM3 (HAVCR2), and CTLA4 was detected in the
321 CD8_Eff group (**Fig 1D**), their levels were low and not significantly different from those in
322 the total cell population.
323 Costimulatory receptors 4-1BB (TNFRSF9), ICOS, CD27, HVEM (TNFRSF14), and
324 LIGHT (TNFSF14) were observed in the CD8_Eff group (**Fig 1D**). LIGHT and ICOS
325 expression were upregulated in all activated BATs groups but were not significantly

326 upregulated in the CD8_Eff group (**Fig 1D**). CD27 was present but downregulated
327 compared to other CD8 groups (**Fig 1D**), indicating terminal effector differentiation[39]. Only
328 4-1BB expression was significantly upregulated in the CD8_Eff group (See **Discussion**).
329 While LAG3 expression was observed throughout the CD8_Eff group, TIGIT expression
330 was concentrated within a subset of these cells (**Fig 1E, F**). Comparison between
331 $TIGIT_{High}$ and $TIGIT_{Low}$ CD8_Eff cells reveals distinct expression of regulatory genes
332 associated with T cell effector differentiation. $TIGIT_{High}$ CD8_Effs are enriched for EOMES
333 and CMC1, while $TIGIT_{Low}$ CD8_Effs are enriched for HOPX and SPRY1. All four genes
334 are involved in T cell effector differentiation37,41–43, but the absence of overlap may
335 indicate a potential divergence in function between $TIGIT_{High}$ and $TIGIT_{Low}$ CD8_Eff cells.
336 These expression patterns may indicate that highly cytotoxic CD8 BATs are more strongly
337 regulated by TIGIT or LAG3 after initial interaction with breast cancer tumor cells and
338 might benefit from CPI therapies targeting these receptors. Likewise, 4-1BB agonism may
339 provide costimulatory signals preferentially to a highly cytotoxic subpopulation.
340

341 **Temporal profiling reveals distinct dynamics of costimulatory and inhibitory**
342 **receptor expression following tumor exposure**

343 The emergence of therapeutically targetable cosignaling receptors as marker genes for
344 highly cytotoxic effector cells after 1 hour of exposure suggests promising potential for
345 effective combinatorial BATs therapies. To determine whether the observed expression
346 patterns of TIGIT, LAG3 and 4-1BB from CITE-seq data persist beyond 1 hour of
347 stimulation – and whether transcriptomic expression patterns translate to expression of
348 surface proteins – we analyzed surface receptor expression on BATs cocultured with HR+

349 breast cancer cell lines. The coexpression dynamics of inhibitory and stimulatory
350 receptors on BATs were profiled over a 72-hour coculture with HR+ tumor cells (**Fig 2A**).
351 Flow cytometry panels used to profile receptor expression are detailed in **Table 1**.
352
353 *CD4 BATs preferentially express PD-1, which coexpresses with LAG3 and TIGIT*
354 CD4 BATs expressed PD-1, TIGIT, and LAG3 during the initial 72-hour challenge (**Fig**
355 **2B**). CD4 BATs preferentially expressed PD-1, while LAG3 and TIGIT were primarily
356 coexpressed on PD-1 expressing cells (**Fig 2E**). ICOS expression within the CD4 pool
357 gradually increased with time, while CD27 expression dipped over 24h before rebounding
358 (**Fig S2**). Th1 CD4 cells expressed PD-1 significantly higher than other BATs groups in
359 our CITE-seq data, potentially suggesting the immediate emergence of a Th1 CD4 subset
360 (**Fig 1D**). Th1 CD4 cells expressed PD-1 significantly higher than other BATs groups in
361 our CD4 data, potentially suggesting the immediate emergence of a Th1 CD4 subset.
362
363 *CD8 BATs rapidly express LAG3 and 4-1BB while gradually increasing PD-1 and TIGIT*
364 *expression*
365 The inhibitory panel showed that CD8 BATs preferentially expressed LAG3 (**Fig 2 B, C**).
366 TIGIT and PD-1 were observed to a lesser extent on CD8 T cells, and primarily
367 coexpressed with LAG3 (**Fig 2 C, E**). TIM3, CTLA4, and BTLA were minimally expressed
368 by BATs over the 72 hours duration of the experiment. In all samples, LAG3+ CD8 BATs
369 hit a proportional and numerical high between 24 and 48 hours after coculture, before
370 declining across the remaining assay duration. PD-1 and TIGIT expression gradually
371 increased as the assay progressed. Interestingly, samples that maintained a higher

372 proportion of LAG3+ CD8 T cells throughout the assay cleared a greater proportion of
373 tumor cells cumulatively across 72 hours. A stimulatory receptor profile demonstrated
374 CD8 BATs primarily expressed 4-1BB and ICOS, with 4-1BB spiking rapidly during the
375 first 24h before exiting the system and ICOS gradually increasing with time. CD27 which
376 was strongly expressed at t = 0 hours, rapidly decreased in expression during the first 24
377 hours, before recovering to initial expression levels during the last 48 hours of the
378 experiment (**Fig S2**). The presence of LAG3, TIGIT, and 4-1BB indicates the CD8 BATs
379 are primarily the CD8_Eff phenotype observed in our CITE-seq data.
380 A coexpression panel was designed to explore overlap between costimulatory and
381 inhibitory receptors (**Fig 2D, F**). Expression of coinhibitory receptors reflected what was
382 observed on the inhibitory panel – LAG3 and PD1 expression dominated CD8 and CD4
383 BATs, respectively, with both PD-1 and TIGIT coexpressing with LAG3 at increasing
384 frequency on CD8s (**Fig 2D, F**). PD-1 and TIGIT rarely coexpressed on CD8s in the
385 absence of LAG3. Interestingly, 4-1BB strongly coexpressed with LAG3 on CD8s during
386 the first 24h (**Fig 2D, F**). LAG3 and 4-1BB presence simultaneously peaked at 24 hours,
387 and LAG3 and TIGIT remained the primary inhibitory receptors after 24 hours, (**Fig 2D,**
388 **F**), which suggests that 4-1BB expression or stimulation precedes T cell activation
389 pathways that preferentially express LAG3 and/or TIGIT.
390
391 **Multivariate statistical analysis predicts opposing effects of LAG3 and TIGIT**
392 **expression on BATs-mediated tumor cell cytotoxicity rates**
393 We hypothesized that LAG3, TIGIT, and PD-1 represent distinct anti-tumor functional
394 phenotypes, with their expression kinetics closely correlating with changes in BATs

395 function and phenotype. PD-1 was enriched in activated Th1 and Th2 CD4 subgroups but
396 did not associate strongly with CD8_Eff in our CITE-seq data (**Fig 1D**). LAG3 and TIGIT
397 correlated strongly with components of cytotoxic pathways in our CITE-seq data (**Fig 1D**)
398 and suggests a highly cytotoxic activated effector state in BATs. However, TIGIT was only
399 partially enriched within our CD8_Eff group and correlated with regulatory components
400 associated with effector cell maturation (**Fig 1D**). A Partial Least Squares Regression
401 (PLS-R) model was constructed to determine if tumor cell reduction cytotoxicity could be
402 predicted by receptor presence (**Fig 3A, B**). Cells were binned by CD4/CD8, TIGIT,
403 LAG3, and PD-1 expression, with cells expressing combinations of these receptors put in
404 unique bins. The prevalence of each phenotype at each timepoint was used to predict the
405 rate of tumor cytotoxicity measured by RTCA at 4 hours post-receptor measurement. Our
406 model predicted 98% of the variance seen in the rate of tumor growth and reduction, and
407 outperformed 1000 random permutations of the data ($p < 0.001$) (**Fig. 3A**). Examining the
408 top predictors of the cytotoxicity, which were defined as those with VIP >1, we observed
409 that CD8 BATs expressing LAG3 with or without PD-1 correlated with increased rates of
410 cytotoxicity, while TIGIT expression on either CD8 or CD4 cells was negatively correlated
411 with the rate of cytotoxicity (**Fig. 3 B, C**). Cells expressing a combination of LAG3 and
412 TIGIT, regardless of PD-1 expression, were not predictive. Cells expressing none of the
413 three receptors were negatively correlated with cytotoxicity, similar to TIGIT expressing
414 cells, potentially suggesting a pre-activated state. In summary, our data show that the
415 expression of LAG3 on BATs is significantly associated with anti-tumor cytotoxicity, while
416 TIGIT expression dampens BATs-driven cytotoxicity (**Fig. 3C**).
417

418 **Mechanistic modeling identifies LAG3 BATs as key drivers of tumor reduction**

419 The PLS-R model indicates that the balance of BATs subsets defined by receptor
420 expression plays a crucial role in tumor reduction. To more directly determine the
421 functional impact of each subset and validate our PLS-R findings, an ODE-based dynamic
422 model of tumor-BATs interactions was constructed (See Methods). Surviving tumor cell
423 counts were extracted from RTCA data, while BATs subset counts were extracted from
424 receptor expression measured by the coexpression flow cytometry panels. Given the
425 homogeneity in CD4 population dynamics across experiments, cytotoxic CD8 cells were
426 selected for the development of the model. Cytotoxic potential as predicted for each
427 subset by the PLS-R model was used to define four functional groups in the kinetic-
428 dynamic BATs-tumor model. Specifically, the PLS-R model predicted LAG3 and TIGIT
429 expression have significant but opposing effects on the rate of tumor expansion or
430 survival. LAG3 expression predicts higher rates of tumor reduction, while TIGIT predicts
431 weaker tumor reduction. The expression of PD-1 was not predictive. Based on the above
432 findings, a mechanistic model of tumor-BATs interactions was constructed consisting of
433 tumor cells and 4 receptor-defined BATs species: LAG3-/TIGIT- BATs (NBATs),
434 LAG3+/TIGIT- BATs (LBATs), LAG3-/TIGIT+ BATs (TBATs), and LAG3+/TIGIT+ BATs
435 (DBATs) (**Fig 4A**).

436 Our ODE model was constructed and distinct cytotoxicity rates were estimated for each
437 BATs phenotype, accurately replicating tumor cell count dynamics over a 72-h BAT-tumor
438 coculture. Tumor growth rates were determined by fitting experimental tumor growth data
439 to sigmoidal curves, using maximum cell counts observed in tumor-only control
440 conditions. Experimentally collected BATs counts were modeled using spline functions to

441 represent dynami changes in BATs numbers over time. CaliPro, an iterative parameter
442 optimization package, was employed to estimate the cytotoxicity parameter space. Value
443 ranges for cytotoxicity rates for each BAT phenotype were identified to best match
444 experimental BATs-tumor dynamics (**Fig 4B**). Finally, estimated cytotoxicity rates and the
445 total number of tumor cells killed by each BATs subpopulation were compared as key
446 metrics to evaluate the cytotoxic potential of each cell phenotype.
447 When comparing a single donor across 3 HER2-/HR+ breast cancer cell lines, LBATs
448 emerge as the clear driver of cytotoxicity (**Table 2** and **Fig 4C**). LBATs demonstrate a
449 larger capacity for tumor clearance both through a higher cytotoxicity rate (**Table 2**) and
450 greater number of tumor cells removed compared to all other species (**Fig. 4C**). This
451 model prediction matches the functional potential observed in our PLS-R model, where
452 LAG3+ BATs correlated with
453 greater tumor reduction (**Fig**
454 **3B**), and our CITE-seq data,
455 where LAG3+ CD8_Eff cells
456 expressed significantly higher
457 granzyme and perforin
458 concentrations than other
459 observed groups (**Fig 1D**). Both factors make the generation of these cells highly
460 desirable therapeutically. Additionally, LAG3+ BATs were observed to proliferate strongly
461 in all systems, indicating they can sustain an effective anti-tumor response when
462 generated. DBATs, which expressed both LAG3 and TIGIT, were observed to also
463 contribute to cytotoxicity, although at a lower rate than LBATs (**Fig 4C**). NBATs were

Parameter	Target		
	MCF7	CAMA1	T47D
Tumor growth rate	0.13	0.06	0.16
Max conductivity	1.4	3.2	1.2
LBAT Cytotoxicity Rate (Range)	1.18E-06 (1.01E-06 - 1.34E-06)		
NBAT Cytotoxicity Rate (Range)	1.95E-07 (1.31E-07 - 1.97E-07)		
DBAT Cytotoxicity Rate (Range)	9.54E-07 (6.61E-07 - 9.63E-07)		
DBAT Cytotoxicity Rate (Range)	9.54E-07 (6.61E-07 - 9.63E-07)		

Table 2: Optimal parameters and ranges determined by CaliPro meeting pass criteria for Donor 1 BATs challenged against 3 tumor cell lines.

464 5.75-fold less cytotoxic than LBATs, although their presence as the most populous BAT
465 subtype meant they contributed significantly to tumor removal. TBATs demonstrated
466 significantly lower cytotoxicity compared to either LAG3+ subgroups LBATs or DBATs
467 and remained at low enough numbers to contribute minimally to tumor reduction.
468 Comparisons across donors revealed consistent patterns of cytotoxicity. While the
469 behavior of BATs derived from different donors could not be described using identical
470 parameter sets, individual models predicted LBATs as the most cytotoxic subset, followed by DBATs, with NBATs and TBATs alternating as the least and second least cytotoxic subgroup (**Fig 5B-C, Table 3**).

Parameter	Donor		
	Donor 1	Donor 2	Donor 3
Tumor growth rate	0.0748		
Max conductivity	7.6		
LBAT Cytotoxicity Rate (Range)	1.18E-06 (1.01E-06 - 1.34E-06)	8.59E-06 (8.38E-06- 1.16E-05)	5.28E-06 (3.89E-06 - 5.95E-06)
NBAT Cytotoxicity Rate (Range)	1.95E-07 (1.31E-07 - 1.97E-07)	4.48E-08 (2.17E-08 - 4.91E-08)	4.49E-07 (5.61E-08 - 7.48E-07)
DBAT Cytotoxicity Rate (Range)	9.54E-07 (6.61E-07 - 9.63E-07)	3.71E-06 (7.90E-07 - 4.35E-06)	1.33E-06 (1.27E-06 - 5.52E-06)
TBAT Cytotoxicity Rate (Range)	3.98E-07 (3.23E-07 - 4.25E-07)	8.59E-08 (5.42E-08 - 5.74E-07)	3.36E-07 (3.34E-07 - 7.31E-07)

Table 3: Optimal parameters ranges determined by CaliPro meeting pass criteria for BATs from three donors challenged against MCF7 tumor cells.

479 Notably, Donor 2, which demonstrated the lowest tumor cell clearance, relied more
480 heavily on its DBATs for tumor reduction. This likely resulted from a higher relative
481 abundance of DBATs generated during the coculture experiment compared to Donors 1
482 and 3.
483 Across all donors, LAG3 emerged as a robust indicator of effector cytotoxicity, suggesting
484 that the LAG3+ CD8 BATs subset plays a primary role in tumor elimination during HR+

486 breast cancer-HER2 targeted BATs immunotherapy In contrast, TIGIT expression in
487 BATs cells may act as a suppressor of cytotoxic function.
488
489 **DISCUSSION**
490 Changes in receptor expression as a function of differentiation likely reflect the T cell's
491 capacity to mount diverse and multifunctional immune responses against perceived
492 threats. Understanding how these phenotypes emerge, and function can significantly
493 enhance our ability to engineer T cells for predictable and effective responses against
494 tumors or pathogens. In this study, we characterized emerging T cell subtypes in BATs
495 challenged by HR+ breast cancers and developed a model combining T cell inhibitory
496 receptor expression dynamics with cytotoxicity rates to identify associations between
497 targetable pathways of T cell inhibition and T cell anti-tumor cytotoxicity.
498 While inhibitory receptor expression is intrinsically linked with T cell stimulation, the
499 factors driving differential expression remain unclear[42–44]. Across three donors and when
500 challenged with 3 HR+ breast cancer cell lines, only TIGIT, LAG3, and PD-1 were
501 expressed within the first 72 hours of challenge. This suggests that combinatorial
502 therapies pairing BATs with CPI therapies should prioritize these receptors.
503 Our model indicates an association between TIGIT surface expression and reduced BATs
504 function. Because TIGIT ligands PVR, NECTIN1, and NECTIN2 have been detected in
505 breast cancer and correlate with poor prognostic outcomes, the loss of function in TIGIT+
506 cells may result of TIGIT-ligand driven inhibition[45,46]. Blocking TIGIT may reverse the
507 suppressive regulatory effect and augment the cytotoxicity of TIGIT+ and LAG3+/TIGIT+
508 subset of BATs. However, TIGIT presence on T cells may indicate a more terminally

509 differentiated and exhausted state. Coexpression of TIGIT with other inhibitory receptors,
510 including PD-1 and LAG3, is a hallmark of T cell dysfunction in tumors[47–50]. Because we
511 observe TIGIT expression primarily in tandem with PD-1 or LAG3, these cells may be
512 terminally exhausted and less capable of mediating cytotoxic activity even if TIGIT
513 activation or activity is blocked.
514 LAG3+ cells do not appear to be inhibited in our model. LAG3 expression in the absence
515 of other inhibitory receptors, such as TIGIT or TIM-3, is a hallmark of cytotoxic effector T
516 cell activation[51–53]. LAG3 has been observed as primarily regulating effector functions like
517 cytotoxicity for tumor-targeting T cells, and thus LAG3 expression by BATs may indicate
518 a highly functional effector group[54,55]. These studies also observe PD-1 as primarily
519 responsible for inhibiting cell proliferation, and thus the lack of PD-1 on our LAG3+
520 population may facilitate the proliferation observed in this population. The primary LAG3
521 ligand, MHC-II, is expressed predominantly on antigen-presenting cells (APCs), and thus
522 should not be present in our coculture system[56]. However, as breast cancers can be
523 enriched in APCs, including pro-tumor macrophages, LAG3+ BATs may encounter strong
524 inhibition when applied in vivo[57,58]. Thus, preemptive blockade of LAG3 may ensure these
525 primary cytotoxic cells maintain their function in patients, regardless of APC presence.
526 Additionally, LAG3 has been observed to inhibit T cell cytotoxicity without stimulation[59].
527 Thus, LAG3 blockade may improve BATs function regardless of APC presence.
528 Our investigation was limited to the dynamic changes in T cell behavior, without capturing
529 tumor cell ligand expression dynamics. We assumed that components governing the rate
530 of interaction between BATs and target cells remain constant, except for changing
531 cytotoxicity observed in different BATs phenotypes. Furthermore, our coculture system

532 was focused strictly on BiAb-mediated CD8 T cell-tumor interactions and studying signals
533 and secreted factors from other cells was beyond the scope of our work. These factors
534 can influence tumor and T cell behaviors affecting cytotoxicity. TCR-activated CD4 and
535 CD8 T cells are known to produce cytokines and other signaling molecules, including
536 interferon gamma (IFNγ) and tumor necrosis factor (TNFα)[60–62], which affect both T cell
537 function and tumor proliferation[63], and were highly expressed in our CD8_Eff group. While
538 the effect of these cytokines may be captured by the cytotoxicity rates predicted in our
539 model, any compounding effects of their persistent presence or increasing concentration
540 may have not been captured by our model. Limiting the model to CD8 T cells might
541 explain the donor-to-donor variability observed in subset-specific tumor clearance rates
542 (**Table 3**). Notably, the initial BAT population for Donor 2 had a much higher proportion
543 of CD4 T cells compared to Donors 1 and 3 and cleared much fewer target cells (**Fig S3**).
544 Donor 2 also began with and generated fewer LAG3+ CD8s, and an increased CD4
545 presence demands fewer CD8s, so this observation may simply be the result of fewer
546 cytotoxic BATs present. However, CD8 BATs expansion was also lower with higher CD4,
547 and particularly PD-1+ CD4, presence, possibly indicating an inhibitory effect elicited from
548 CD4 BATs. The inclusion of other effector cells might further improve the model fits (**Fig**
549 **5A**).
550 Target cell phenotypic changes also likely change BATs-target interactions but are not
551 captured in our system. Cytokine presence and cell damage can change receptor
552 expression on target cells in a manner that may alter BATs-target interactions with time.
553 Inflammatory cytokines, and in particular Type I interferons, can upregulate inhibitory
554 receptor expression on T cells[64]. Similarly, IFNγ can upregulate cognate ligands for

555 inhibitory receptors, such as PD-L1, on tumor cells[65]. Cell damage and tumor mutational
556 status can also upregulate these ligands[66–68]. Expression of PVR, a TIGIT ligand, has
557 been observed in response to DNA damage, and may be present on some or all the target
558 cells in our system[69]. Thus, the target cells in our system may evolve to inhibit BATs
559 expressing certain inhibitory receptors.
560 Preferential generation of more cytotoxic BATs subspecies may improve tumor clearance
561 against HR+ breast cancers. Costimulatory signaling is a crucial part of T cell activation
562 and plays a role in inhibitory receptor expression intensity[70,71]. Both our CITE-seq and
563 flow cytometry data indicate 4-1BB expression is associated with cytotoxic effector BATs.
564 4-1BB was observed to be strongly correlated with LAG3+/TIGIT+ CD8_Eff cells in our
565 CITE-seq data (**Fig 1D**), and 4-1BB ligand expression was strongly correlated with LAG3
566 and TIGIT expression for the initial 24h of our coculture experiment before disappearing
567 from our system (**Fig 2D, Fig S2**). This may indicate that 4-1BB exists to stimulate highly
568 cytotoxic BATs upon their initial encounter with target cells. However, it is unclear if 4-
569 1BB stimulation is associated with TIGIT expression alone, or if it is also linked to LAG3
570 expression. Further exploration of the impact of 4-1BB stimulation on BATs function and
571 inhibitory receptor expression may provide insight into what incoming signals govern
572 BATs function. If 4-1BB activation changes BATs function, whether to increase or
573 decrease cytotoxicity, utilization of 4-1BB targeting therapies may enhance tumor
574 reduction. A small number of 4-1BBL+ BATs were observed in our system at 4 hours,
575 which may be indicative of a self-stimulating T cell subtype previously observed to
576 increase tumor kill in mouse breast cancer models[72]. However, the transient nature of
577 both 4-1BB and 4-1BBL makes their utilization as targets difficult.

578 Together, these findings provide a compelling support for the use of predictive statistical
579 analysis and mathematical modeling in the rational design of combination
580 immunotherapies. They also strongly suggest that the anti-solid tumor activity of BATs in
581 our phase I/II metastatic breast cancer clinical trials may be in part driven by the
582 dominance of a LAG3+ cytotoxic phenotype over TIGIT downregulatory activity[12,13]. Our
583 recent phase II trial in hormone refractory prostate cancer (HRPC) that combines the CPI
584 pembrolizumab with HER2 targeted BATs showed significant clinical improvement in
585 clinical responses and improved survival[73] when the use of CPI alone has not been
586 successful in clinical test for HRPC. Furthermore, our recent ongoing trial combining
587 pembrolizumab with HER2 BATs in selected metastatic breast cancer patients heavily
588 pretreated with chemotherapy led to stable disease and improved survival (unpublished).
589 The improvement in patient response to BATs combined with a PD-1/PD-L1 targeting
590 therapy bodes well for further work in this area: our model predicted PD-1 to have a lower
591 impact on BATs function than LAG3 or TIGIT and thus combining BATs with a LAG3 or
592 TIGIT blockade may improve responses to an even greater extent. Further investigations
593 into CPI and BATs combination strategies targeting stimulatory or inhibitory receptors to
594 enhance BATs effector functions will likely improve the potential of BATs therapy in
595 metastatic breast cancers and other solid tumors.

596 **REFERENCES**

597 1. Giaquinto, A. N. *et al.* Breast Cancer Statistics, 2022. *CA Cancer J Clin* **72**, 524–541
598 (2022).
599 2. Albarrán, V. *et al.* Adoptive T cell therapy for solid tumors: current landscape and future
600 challenges. *Front Immunol* **15**, 1352805 (2024).
601 3. Helmich, B. K. & Dutton, R. W. The role of adoptively transferred CD8 T cells and host
602 cells in the control of the growth of the EG7 thymoma: factors that determine the relative
603 effectiveness and homing properties of Tc1 and Tc2 effectors. *J Immunol* **166**, 6500–6508
604 (2001).
605 4. Lee, H. J. *et al.* Expansion of tumor-infiltrating lymphocytes and their potential for
606 application as adoptive cell transfer therapy in human breast cancer. **8**, 113345–113359
607 (2017).
608 5. Lum, L. G. *et al.* Clinical and immune responses to anti-CD3 x anti-EGFR bispecific
609 antibody armed activated T cells (EGFR BATs) in pancreatic cancer patients.
610 *Oncoimmunology* **9**, (2020).
611 6. Grabert, R. C. *et al.* Human T Cells Armed with Her2/neu Bispecific Antibodies Divide,
612 Are Cytotoxic, and Secrete Cytokines with Repeated Stimulation Cancer Therapy:
613 Preclinical. *Clin Cancer Res* **12**, (2006).
614 7. Lum, L. G. *et al.* CD20-targeted T cells after stem cell transplantation for high risk and
615 refractory non-Hodgkin's lymphoma. *Biol Blood Marrow Transplant* **19**, 925–933 (2013).
616 8. Thakur, A. *et al.* Immune T cells can transfer and boost anti-breast cancer immunity.
617 *Oncoimmunology* **7**, (2018).
618 9. Lum, L. G. *et al.* Targeted T-cell therapy in stage IV breast cancer: A phase i clinical
619 trial. *Clinical Cancer Research* **21**, 2305–2314 (2015).
620 10. Davol, P. A., Smith, J. A., Kouttab, N., Elfenbein, G. J. & Lum, L. G. Anti-CD3 × Anti-
621 HER2 Bispecific Antibody Effectively Redirects Armed T Cells to Inhibit Tumor
622 Development and Growth in Hormone-Refractory Prostate Cancer–Bearing Severe Combined
623 Immunodeficient Beige Mice. *Clin Prostate Cancer* **3**, 112–121 (2004).
624 11. Yankelevich, M. *et al.* Targeting refractory/recurrent neuroblastoma and osteosarcoma
625 with anti-CD3×anti-GD2 bispecific antibody armed T cells. *J Immunother Cancer* **12**,
626 e008744 (2024).
627 12. Lum, L. G. *et al.* Targeted T-cell therapy in stage IV breast cancer: A phase i clinical
628 trial. *Clinical Cancer Research* **21**, 2305–2314 (2015).
629 13. Lum, L. G. *et al.* Phase II clinical trial using anti-CD3 × anti-HER2 bispecific antibody
630 armed activated T cells (HER2 BATs) consolidation therapy for HER2 negative (0–2+)
631 metastatic breast cancer. *J Immunother Cancer* **9**, e002194 (2021).
632 14. Rugo, H. S. *et al.* Safety and Antitumor Activity of Pembrolizumab in Patients with
633 Estrogen Receptor-Positive/Human Epidermal Growth Factor Receptor 2-Negative Advanced
634 Breast Cancer. *Clin Cancer Res* **24**, 2804–2811 (2018).
635 15. Cardoso, F., Jia, L., Hirshfield, K. & Karantza, V. KEYNOTE-756: Randomized, double-
636 blind, phase III study of pembrolizumab vs placebo + neoadjuvant chemotherapy (CT) and
637 adjuvant endocrine therapy (ET) for high-risk, early-stage estrogen receptor–positive human
638 epidermal growth factor receptor 2–negative (ER+/HER2−) breast cancer (BC). *Annals of*
639 *Oncology* **30**, iii38 (2019).
640 16. Dirix, L. Y. *et al.* Avelumab, an anti-PD-L1 antibody, in patients with locally advanced
641 or metastatic breast cancer: a phase 1b JAVELIN Solid Tumor study. *Breast Cancer Res*
642 *Treat* **167**, 671–686 (2018).

643 17. Rotte, A., Jin, J. Y. & Lemaire, V. Mechanistic overview of immune checkpoints to
644 support the rational design of their combinations in cancer immunotherapy. *Ann Oncol* **29**,
645 71–83 (2018).
646 18. Goleva, E. *et al.* Our current understanding of checkpoint inhibitor therapy in cancer
647 immunotherapy. *Ann Allergy Asthma Immunol* **126**, 630–638 (2021).
648 19. Ildefonso, G. V. & Finley, S. D. A data-driven Boolean model explains memory subsets
649 and evolution in CD8+ T cell exhaustion. *npj Systems Biology and Applications 2023 9:1* **9**,
650 1–13 (2023).
651 20. Yan, M. *et al.* Dynamic regulatory networks of T cell trajectory dissect transcriptional
652 control of T cell state transition. *Mol Ther Nucleic Acids* **26**, 1115–1129 (2021).
653 21. Bolouri, H. *et al.* Integrative network modeling reveals mechanisms underlying T cell
654 exhaustion. *Scientific Reports 2020 10:1* **10**, 1–15 (2020).
655 22. Sontag, E. D. A Dynamic Model of Immune Responses to Antigen Presentation Predicts
656 Different Regions of Tumor or Pathogen Elimination. *Cell Syst* **4**, 231-241.e11 (2017).
657 23. Cess, C. G. & Finley, S. D. Data-driven analysis of a mechanistic model of CAR T cell
658 signaling predicts effects of cell-to-cell heterogeneity. *J Theor Biol* **489**, 110125 (2020).
659 24. Uberti, J. P. *et al.* Preclinical Studies Using Immobilized OKT3 to Activate Human T
660 Cells for Adoptive Immunotherapy: Optimal Conditions for the Proliferation and Induction of
661 Non-MHC-Restricted Cytotoxicity. *Clin Immunol Immunopathol* **70**, 234–240 (1994).
662 25. Sen, M. *et al.* Use of Anti-CD3 × Anti-HER2/neu Bispecific Antibody for Redirecting
663 Cytotoxicity of Activated T Cells Toward HER2/neu+ Tumors.
664 *https://home.liebertpub.com/scd* **10**, 247–260 (2004).
665 26. Stoeckius, M. *et al.* Simultaneous epitope and transcriptome measurement in single cells.
666 *Nature Methods 2017 14:9* **14**, 865–868 (2017).
667 27. Hao, Y. *et al.* Dictionary learning for integrative, multimodal and scalable single-cell
668 analysis. *Nature Biotechnology 2023 42:2* **42**, 293–304 (2023).
669 28. Thakur, A. *et al.* Priming of pancreatic cancer cells with bispecific antibody armed
670 activated T cells sensitizes tumors for enhanced chemoresponsiveness. *Oncoimmunology* **10**,
671 (2021).
672 29. Chong, I. G. & Jun, C. H. Performance of some variable selection methods when
673 multicollinearity is present. *Chemometrics and Intelligent Laboratory Systems* **78**, 103–112
674 (2005).
675 30. Joslyn, L. R., Kirschner, D. E. & Linderman, J. J. CaliPro: A Calibration Protocol That
676 Utilizes Parameter Density Estimation to Explore Parameter Space and Calibrate Complex
677 Biological Models. doi:10.1007/s12195-020-00650-z.
678 31. Guo, M., Liu, M. Y. R. & Brooks, D. G. Regulation and impact of tumor-specific CD4+
679 T cells in cancer and immunotherapy. *Trends Immunol* **45**, 303–313 (2024).
680 32. Zheng, L. *et al.* Pan-cancer single-cell landscape of tumor-infiltrating T cells. *Science*
681 *(1979)* **374**, (2021).
682 33. Correia, M. P. *et al.* Distinct human circulating NKp30+FceRIγ+CD8+ T cell population
683 exhibiting high natural killer-like antitumor potential. *Proc Natl Acad Sci U S A* **115**, E5980–
684 E5989 (2018).
685 34. Garner, L. C. *et al.* Single-cell analysis of human MAIT cell transcriptional, functional
686 and clonal diversity. *Nature Immunology 2023 24:9* **24**, 1565–1578 (2023).
687 35. Lu, B. *et al.* IL-17 production by tissue-resident MAIT cells is locally induced in children
688 with pneumonia. *Mucosal Immunol* **13**, 824–835 (2020).

689 36. Intlekofer, A. M. *et al.* Effector and memory CD8+ T cell fate coupled by T-bet and
690 eomesodermin. *Nature Immunology 2005 6:12* **6**, 1236–1244 (2005).
691 37. Willinger, T. *et al.* Human Naive CD8 T Cells Down-Regulate Expression of the WNT
692 Pathway Transcription Factors Lymphoid Enhancer Binding Factor 1 and Transcription
693 Factor 7 (T Cell Factor-1) following Antigen Encounter In Vitro and In Vivo. *The Journal of*
694 *Immunology* **176**, 1439–1446 (2006).
695 38. Khan, O. *et al.* TOX transcriptionally and epigenetically programs CD8+ T cell
696 exhaustion. *Nature 2019 571:7764* **571**, 211–218 (2019).
697 39. Bullock, T. N. Stimulating CD27 to quantitatively and qualitatively shape adaptive
698 immunity to cancer. *Curr Opin Immunol* **45**, 82–88 (2017).
699 40. Dominguez, C. X. *et al.* The transcription factors ZEB2 and T-bet cooperate to program
700 cytotoxic T cell terminal differentiation in response to LCMV viral infection. *Journal of*
701 *Experimental Medicine* **212**, 2041–2056 (2015).
702 41. Shan, Q. *et al.* Runx3 guards cytotoxic CD8+ effector T cells against deviation towards
703 TFH cell lineage. *Nat Immunol* **18**, 931 (2017).
704 42. Thommen, D. S. *et al.* Progression of lung cancer is associated with increased
705 dysfunction of T cells defined by coexpression of multiple inhibitory receptors. *Cancer*
706 *Immunol Res* **3**, 1344–1354 (2015).
707 43. Baitsch, L. *et al.* Extended Co-Expression of Inhibitory Receptors by Human CD8 T-
708 Cells Depending on Differentiation, Antigen-Specificity and Anatomical Localization. *PLoS*
709 *One* **7**, e30852 (2012).
710 44. Li, X. *et al.* A comprehensive analysis of key immune checkpoint receptors on tumor-
711 infiltrating t cells from multiple types of cancer. *Front Oncol* **9**, 472080 (2019).
712 45. Chiang, E. Y. & Mellman, I. TIGIT-CD226-PVR axis: advancing immune checkpoint
713 blockade for cancer immunotherapy. *J Immunother Cancer* **10**, e004711 (2022).
714 46. Boissière-Michot, F. *et al.* Correlation of the TIGIT-PVR immune checkpoint axis with
715 clinicopathological features in triple-negative breast cancer. *Front Immunol* **13**, 1058424
716 (2022).
717 47. Worboys, J. D. *et al.* TIGIT can inhibit T cell activation via ligation-induced
718 nanoclusters, independent of CD226 co-stimulation. *Nature Communications 2023 14:1* **14**,
719 1–21 (2023).
720 48. Liu, Z. *et al.* TIGIT and PD-1 expression atlas predicts response to adjuvant
721 chemotherapy and PD-L1 blockade in muscle-invasive bladder cancer. *British Journal of*
722 *Cancer 2022 126:9* **126**, 1310–1317 (2022).
723 49. Wherry, E. J. & Kurachi, M. Molecular and cellular insights into T cell exhaustion.
724 *Nature Reviews Immunology 2015 15:8* **15**, 486–499 (2015).
725 50. Takamatsu, K. *et al.* Profiling the inhibitory receptors LAG-3, TIM-3, and TIGIT in renal
726 cell carcinoma reveals malignancy. *Nature Communications 2021 12:1* **12**, 1–12 (2021).
727 51. Workman, C. J. & Vignali, D. A. A. The CD4-related molecule, LAG-3 (CD223),
728 regulates the expansion of activated T cells. *Eur J Immunol* **33**, 970–979 (2003).
729 52. Grosso, J. F. *et al.* Functionally Distinct LAG-3 and PD-1 Subsets on Activated and
730 Chronically Stimulated CD8 T Cells. *The Journal of Immunology* **182**, 6659–6669 (2009).
731 53. Kallies, A., Zehn, D. & Utzschneider, D. T. Precursor exhausted T cells: key to
732 successful immunotherapy? *Nature Reviews Immunology 2019 20:2* **20**, 128–136 (2019).

733 54. Ngiow, S. F. *et al.* LAG-3 sustains TOX expression and regulates the CD94/NKG2-Qa-
734 1b axis to govern exhausted CD8 T cell NK receptor expression and cytotoxicity. *Cell* **187**,
735 4336-4354.e19 (2024).
736 55. Andrews, L. P. *et al.* LAG-3 and PD-1 synergize on CD8+ T cells to drive T cell
737 exhaustion and hinder autocrine IFN-γ-dependent anti-tumor immunity. *Cell* **187**, 4355-
738 4372.e22 (2024).
739 56. Baixeras, E. *et al.* Characterization of the lymphocyte activation gene 3-encoded protein.
740 A new ligand for human leukocyte antigen class II antigens. *Journal of Experimental*
741 *Medicine* **176**, 327–337 (1992).
742 57. Williams, C. B., Yeh, E. S. & Soloff, A. C. Tumor-associated macrophages: unwitting
743 accomplices in breast cancer malignancy. *npj Breast Cancer 2016 2:1* **2**, 1–12 (2016).
744 58. Medrek, C., Pontén, F., Jirström, K. & Leandersson, K. The presence of tumor associated
745 macrophages in tumor stroma as a prognostic marker for breast cancer patients. *BMC Cancer*
746 **12**, 1–9 (2012).
747 59. Guy, C. *et al.* LAG3 associates with TCR–CD3 complexes and suppresses signaling by
748 driving co-receptor–Lck dissociation. *Nature Immunology 2022 23:5* **23**, 757–767 (2022).
749 60. Bachmann, M. F., Barner, M., Viola, A. & Kopf, M. Distinct kinetics of cytokine
750 production and cytolysis in effector and memory T cells after viral infection.
751 doi:10.1002/(SICI)1521-4141(199901)29:01.
752 61. Veiga-Fernandes, H., Walter, U., Bourgeois, C., McLean, A. & Rocha, B. Response of
753 naïve and memory CD8+ T cells to antigen stimulation in vivo. *Nature Immunology 2000 1:1*
754 **1**, 47–53 (2000).
755 62. Helmich, B. K. & Dutton, R. W. The role of adoptively transferred CD8 T cells and host
756 cells in the control of the growth of the EG7 thymoma: factors that determine the relative
757 effectiveness and homing properties of Tc1 and Tc2 effectors. *J Immunol* **166**, 6500–6508
758 (2001).
759 63. Dong, C. Cytokine Regulation and Function in T Cells. *Annu Rev Immunol* **39**, 51–76
760 (2021).
761 64. Sumida, T. S. *et al.* Type I interferon transcriptional network regulates expression of
762 coinhibitory receptors in human T cells. *Nature Immunology 2022 23:4* **23**, 632–642 (2022).
763 65. Spranger, S. *et al.* Up-regulation of PD-L1, IDO, and Tregs in the melanoma tumor
764 microenvironment is driven by CD8+ T cells. *Sci Transl Med* **5**, (2013).
765 66. Sato, H. *et al.* DNA double-strand break repair pathway regulates PD-L1 expression in
766 cancer cells. *Nature Communications 2017 8:1* **8**, 1–11 (2017).
767 67. Strickland, K. C. *et al.* Association and prognostic significance of BRCA1/2-mutation
768 status with neoantigen load, number of tumor-infiltrating lymphocytes and expression of PD-
769 1/PD-L1 in high grade serous ovarian cancer. *Oncotarget* **7**, 13587 (2016).
770 68. Rosenbaum, M. W., Bledsoe, J. R., Morales-Oyarvide, V., Huynh, T. G. & Mino-
771 Kenudson, M. PD-L1 expression in colorectal cancer is associated with microsatellite
772 instability, BRAF mutation, medullary morphology and cytotoxic tumor-infiltrating
773 lymphocytes. *Modern Pathology* **29**, 1104–1112 (2016).
774 69. Gorvel, L. & Olive, D. Targeting the "PVR–TIGIT axis" with immune checkpoint
775 therapies. *F1000Res* **9**, (2020).
776 70. Messenheimer, D. J. *et al.* Cancer Therapy: Preclinical Timing of PD-1 Blockade Is
777 Critical to Effective Combination Immunotherapy with Anti-OX40. *Clin Cancer Res* **23**,.

71. Koyama, S. *et al.* Adaptive resistance to therapeutic PD-1 blockade is associated with upregulation of alternative immune checkpoints. *Nature Communications 2016 7:1* **7**, 1–9 (2016).
72. Cho, E. *et al.* 4-1BB-4-1BBL cis-interaction contributes to the survival of self-reactive CD8+ T cell. *Cellular & Molecular Immunology 2023 20:9* **20**, 1077–1080 (2023).
73. Vaishampayan, U. N. *et al.* Phase II Trial of Pembrolizumab and Anti-CD3 x Anti-HER2 Bispecific Antibody-Armed Activated T Cells in Metastatic Castration-Resistant Prostate Cancer. *Clinical Cancer Research* **29**, 122–133 (2023).

Figure captions

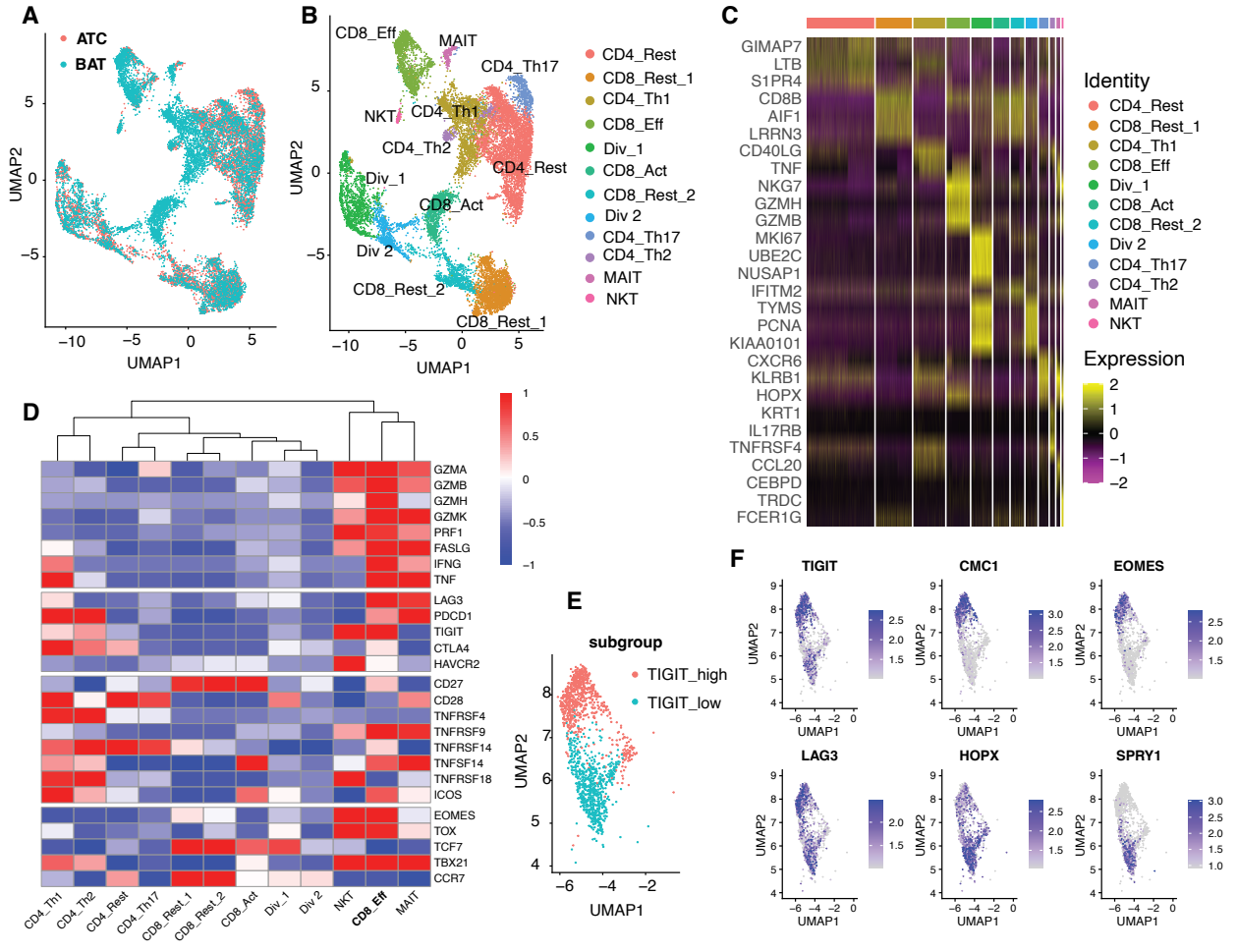

Figure 1:

A: UMAP plot of CITE-seq data labeled by bispecific antibody arming. ATC: unarmed Activated T Cells, BAT: Bispecific antibody-armed Activated T cells

B: A UMAP plot of T cells clustered by similarity in gene expression. Labels were chosen based on expression of significantly upregulated marker genes. CD4_Rest = Resting CD4 T cells; CD8_Rest_1 = Group 1 Resting CD8 T cells; CD4_Th1 = Th1 CD4 T cells; CD8_Eff = Effector CD8 T cells; Div_1 = Group 1 Dividing T cells; CD8_Act = Activated CD8 T cells; CD8_Rest_2 = Group 2 Resting CD8 T cells; Div_2 = Group 2 Dividing T cells; CD4_Th17 = Th17 CD4 T cells; CD4_Th2 = Th2 CD4 T cells; MAIT = Mucosal Associated Invariant T cells; NKT = NK-like T cells

C: Heatmap of most differentially expressed genes as determined by a Wilcoxon ranked sum test. Genes shown most strongly differentiate each group from all other groups and were used to determine the labels in 1B.

D: A heat map of average gene expression scaled across groups. Genes displayed are involved in cytotoxicity (top), T cell inhibition (second top), T cell costimulation (second bottom), and T cell maturation and differentiation (bottom).

E: A re-clustered UMAP of effector CD8 T cells.

F: Differentially expressed genes between the two CD8_Eff clusters.

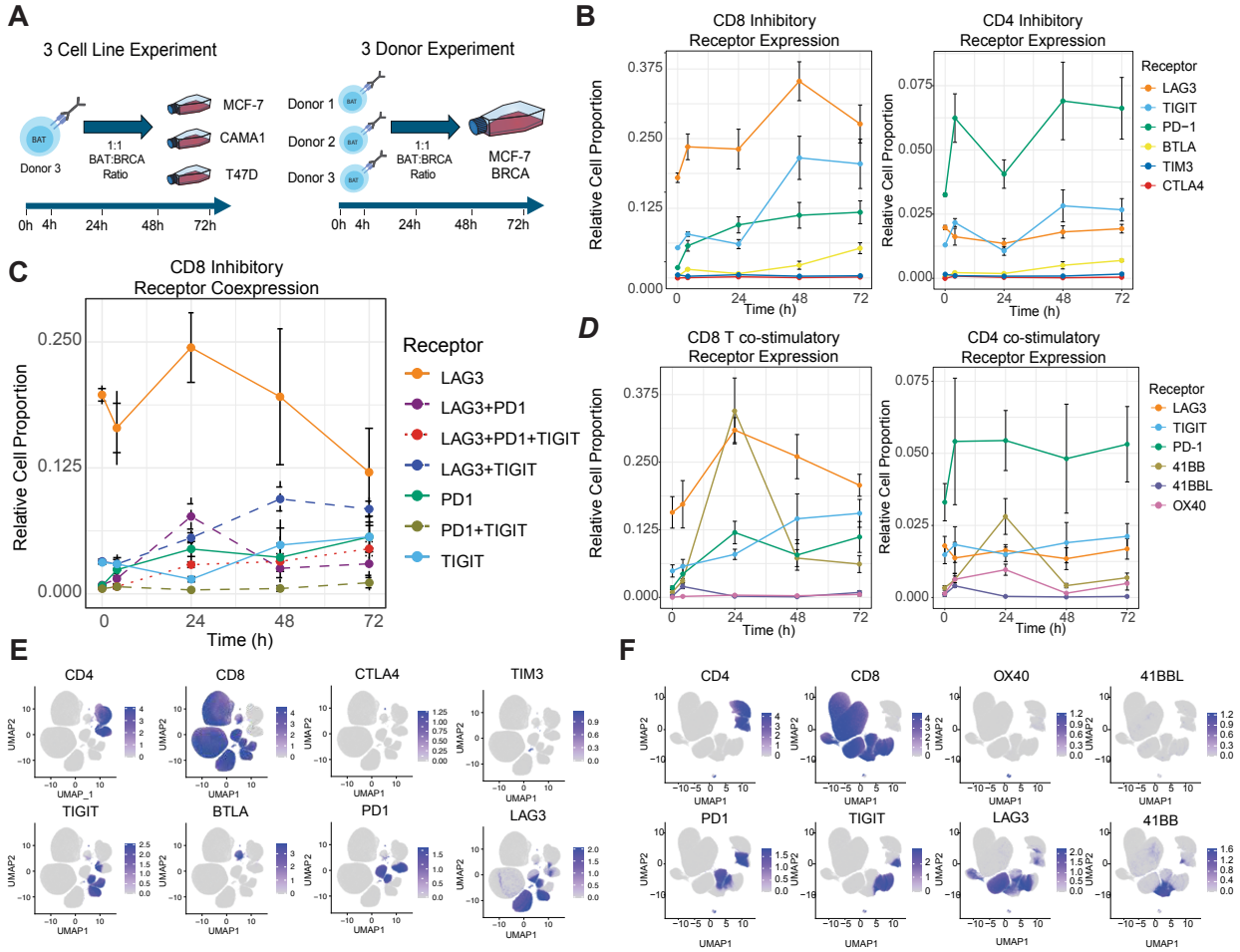

Figure 2:

810 A: Diagram illustrating the setup and data collection for the two sets of flow cytometry experiments
811 performed. Left Panel - BATs generated from Donor 1 challenged against MCF-7, CAMA1, and
812 T47D breast cancer cell lines. Samples collected at 0, 4, 24, 48, and 72 hours and designated '3
813 Cell Line Experiment'. Right Panel - BATs generated from Donors 1, 2, and 3 challenged
814 separately against MCF-7 breast cancer cell line. Samples collected at 0, 4, 24, 48, and 72 hours
815 and designated '3 Donor Experiment'.
816 B: Inhibitory panel receptor expression on CD8 (left panel) and CD4 (right panel) BATs. Data
817 shown was collected from the 3 Cell Line experiment and is presented as the mean value across
818 all cell lines. Error bars indicate standard error within each data group. Each line represents the
819 relative proportion of the cells that express a marker regardless of other marker expression.
820 C: Relative cell proportion of CD8 cells expressing LAG3, TIGIT, PD-1, or a combination thereof.
821 Cells were binned specificly by their expression or combination of expression of LAG3, TIGIT,
822 and PD-1. Unlike Panels B and D, there is no overlap between groups containing a common
823 ligand. For example, the TIGIT+ CD8 T cell subset does not express PD-1 or LAG3. Samples
824 collected at 0, 4, 24,48, and 72 hours. Data represents mean value across 3 Cell Line experiment
825 as collected in the coexpression panel. Error bars represent the range within each sample
826 timepoint.
827 D: Coexpression panel receptor expression on CD8 (left panel) and CD4 (right panel) BATs. Data
828 shown was collected from the 3 Cell Line experiment and is presented as the mean value across
829 all cell lines. Error bars indicate standard error within each data group. Each line represents the
830 relative proportion of the cells that express a marker and can have other markers simultaneously
831 expressed.
832 E: UMAP of BAT cells from the 3 Cell Line experiment clustered by receptor expression as
833 measured by flow cytometry in the inhibitory panel.
834 F: UMAP of BAT cells from the Cell Line experiment clustered by receptor expression as
835 measured by flow cytometry in the coexpression panel.

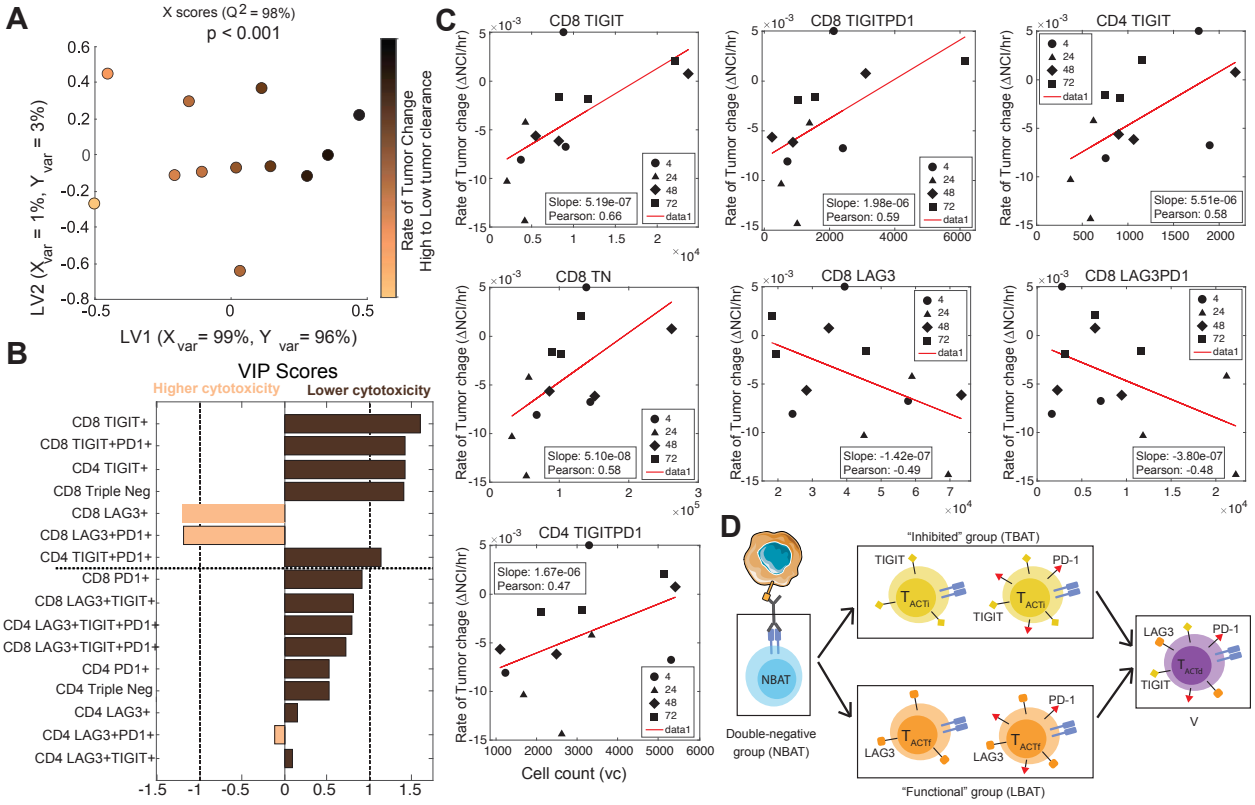

Figure 3:

A: OPLS-R model of rate of tumor change predicted by BAT subpopulations from the 3 Cell Line experiment. BATs were binned by CD4 or CD8 expression, and further binned by expression of LAG3, TIGIT, and/or PD-1. Cells expressing more than one receptor were binned in separate categories, with cells expressing all three receptors being designated tri-positive (TP). BATs lacking receptors were designated tri-negative (TN).

B: VIP scores generated by PLS-R model in Figure 3A. Subpopulation impact is designated by the magnitude of the VIP score, with scores of magnitude >1 designated as greater-than-average contribution of that cell subpopulation to tumor reduction. Subpopulations with scores colored tan are associated with reduced rate of tumor change, while subpopulations with scores colored brown are negatively associated with reduced rate of tumor change.

C: Scatter plots comparing the viable cell count of BAT subpopulations (x-axis) to rate of tumor change (y-axis) for subpopulations with VIP scores >1. NCI = normalized cell index.

850 D: Diagram of BAT developmental progression as assumed by the model. BATs are grouped as
851 NBATs (LAG3-/TIGIT-), LBATs (LAG3+/TIGIT-), TBATs (LAG3-/TIGIT+), or DBATs
852 (LAG3+/TIGIT+). PD-1 expression does not factor into grouping and can be present within any
853 group. These four groups are used to govern tumor reduction in the models presented in Figures
854 4 and 5.

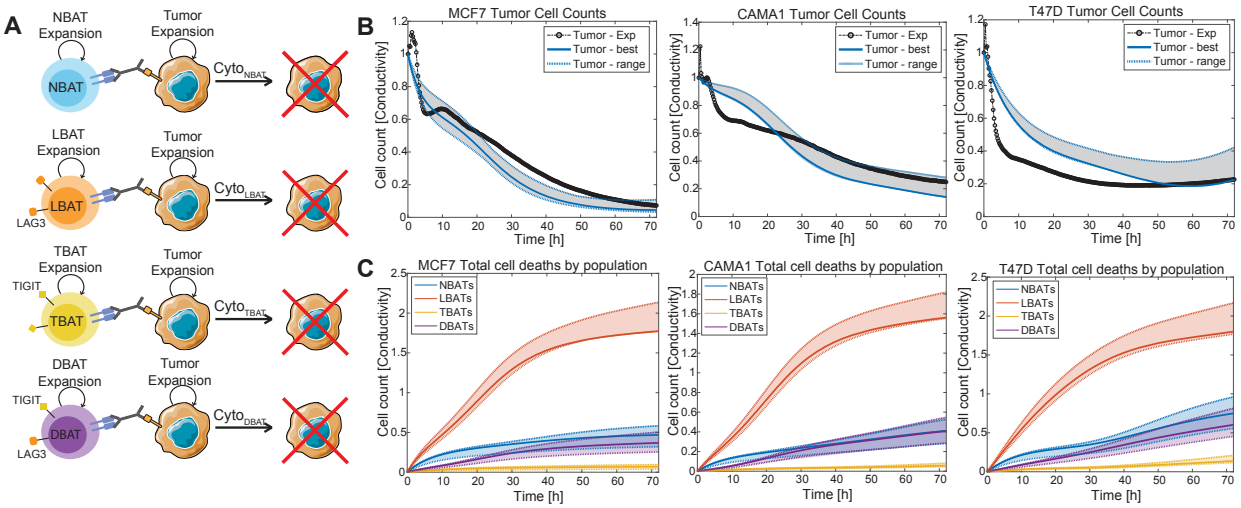

855

856 **Figure 4:**

857 A: Diagram representing processes represented in the model. Tumor expansion parameters were
858 determined by fitting a sigmoidal curve to tumor growth data from control conditions in which BATs
859 were absent. BAT subgroup expansion was fit to individual splines to capture the count data
860 determined from flow cytometry. CaliPro was used to fit cytotoxicity rates for each BAT subgroup
861 to match the experimentally measured BAT and tumor cell counts. Data from the 3 Cancer
862 experiment was used in parameter determination and is shown in B and C.

863 B: MCF-7 (left), CAMA1 (center), and T47D (right) cell counts as measured by RTCA (black) and
864 as predicted by the model (blue). Optimal model prediction in sold blue line, while range of
865 predictions depicted by dotted blue lines.

866 C: MCF-7 (left), CAMA1 (center), and T47D (right) cell reduction by BAT phenotype as predicted
867 by the model. LBAT (orange), NBAT (blue), TBAT (yellow), and DBAT (purple) cumulative

868 reduction is shown for optimal conditions (solid line) and for total range of predictions (dotted

869 lines).

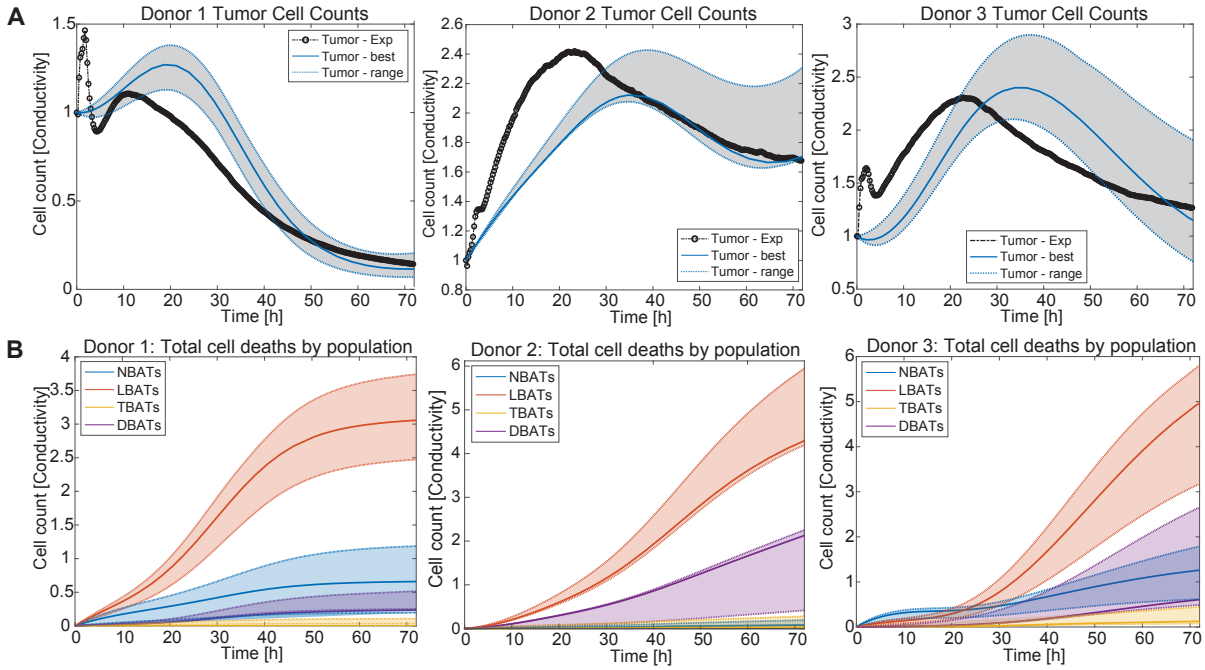

870

871 **Figure 5:**

872 A: MCF-7 cell counts as measured by RTCA (black) and as predicted by the model (blue) when

873 challenged by Donor 1 (left), Donor 2 (middle), and Donor 3 (right) BATs. Optimal model prediction

874 in sold blue line, while range of predictions depicted by dotted blue lines.

875 B: MCF-7 cell reduction by BAT phenotype as predicted by the model when challenged by Donor

876 1 (left), Donor 2 (middle), and Donor 3 (right) BATs. LBAT (orange), NBAT (blue), TBAT (yellow),

877 and DBAT (purple) cumulative reduction is shown for optimal conditions (solid line) and for total

878 range of predictions (dotted lines).

879